Proceedings of the 21st ICSMGE, Vienna, Austria, 14 – 19 June 2026. Pistrol, Adam & Schweiger (eds.)
Published by: ÖGG, Austrian Society for Geomechanics, Salzburg, Austria, ISBN 978-3-9503898-4-5
https://doi.org/10.53243/ICSMGE2026-401

Investigation on seismic response of deeply embedded nuclear island building considering soil-pile-structure interaction

Dong Feng[1], Meng Chu[2], Jie Yang[2], Weiming Gong[1]*, Zhenkun Ding[2], Yu Ren[2], Bing Li[1], Yugang Sun[2]

[1]Key Laboratory of Concrete and Prestressed Concrete Structures of Ministry of Education, College of Civil Engineering, Southeast University, Nanjing 211189, China.
[2]Shanghai Nuclear Engineering Research & Design Institute Co. Ltd., Shanghai 200233, China.
**Corresponding author. E-mail: wmgong@seu.edu.cn*

ABSTRACT: Addressing the seismic technical challenges associated with constructing nuclear power plants on non-rock sites (where shear wave velocity v_s < 1100 m/s), this study delves into the influence mechanisms of soil-pile-structure interaction (SPSI) on the seismic response of deeply embedded nuclear island buildings, aiming to provide a scientific basis for optimizing their seismic design. Employing a combined methodology of large-scale shaking table tests and numerical simulations, the scaled models of nuclear island building supported on different foundations were constructed. An innovative multi-directional laminar shear soil container was developed, enabling the control of container stiffness (with boundary effect index μ < 3.5%) through adjustment of energy-dissipating rod parameters, thereby effectively simulating semi-infinite foundation conditions. Key findings include: The SPSI effect significantly reduces the acceleration amplification of nuclear island building induced by vertical seismic wave propagation, yielding a comprehensive reduction of 14.98% to 27.91%; When the lateral bearing capacity of piled raft foundation is fully mobilized under strong earthquakes, peak bending moments concentrate at the pile heads, and load distribution follows distinct patterns: corner piles > edge piles > center piles, and front-row piles > back-row piles; Implementing a reasonable embedment depth allows for the effective utilization of passive earth pressure constraints, enhancing system energy dissipation and significantly reducing structural seismic response. Test results validated the effectiveness of the established numerical simulation method for the non-rock site–piled raft foundation–reactor building system. This research reveals the key influence mechanisms of SPSI on the seismic response of deeply embedded nuclear island buildings. The proposed analytical methods and embedment depth optimization strategy based on passive earth pressure effects provide crucial technical supports for the seismic safety design of nuclear power plants on non-rock sites.

KEYWORDS: Non-rock site; Nuclear island building; Soil-pile-structure interaction (SPSI); Seismic response; Shaking table test; Passive earth pressure.

1 INTRODUCTION

The seismic safety of nuclear power plants (NPPs) is paramount, as historical events like those at Kashiwazaki-Kariwa and Fukushima NPPs starkly demonstrate (Hidenori et al. 2010; Tang & Schiff, 2010; Uetake et al. 2011; IAEA,2015; Martin, 2018). While stringent siting criteria traditionally favor stable rock foundations to mitigate seismic risk (Yin et al. 2015), the expansion of nuclear power necessitates exploring non-rock sites where suitable rock locations are scarce (Liu et al. 2024; Wang et al. 2024; Hu et al. 2025). Constructing NPPs on these softer soil sites (Class II/III, defined by shear wave velocities v_s < 1100 m/s and v_s < 300 m/s respectively per IAEA (IAEA, 2016), Chinese code (MHUDPRC, 2014), and AP1000 design (Westinghouse Electric Company LLC, 2007)) introduces significant challenges. The dynamic interaction between the deformable soil, foundation, and massive, stiff superstructure – known as soil-structure interaction (SSI), or more specifically for piled foundations, soil-pile-structure interaction (SPSI) – critically influences the seismic response (Mostafa & El Naggar, 2002; Forcellini, 2022 and 2023; Islam et al. 2024). Crucially, designing for non-rock sites by assuming a fixed-base condition (as for rock) can lead to non-conservative or unsafe outcomes (Forcellini, 2022 and 2023), necessitating explicit consideration of SPSI effects as mandated by standards like IAEA (IAEA, 2016) and ASCE/SEI 4-16 (ASCE, 2017).

Piled raft foundations are a common solution for NPPs in non-rock sites to meet bearing capacity, settlement control, and seismic resistance requirements (Clancy & Randolph, 1993; Poulos & Davids, 2005; Sonoda et al. 2009; Zou et al. 2020; Yang et al. 2021). However, the seismic behavior of the integrated soil-piled raft-NPP superstructure system remains complex. SPSI involves intricate kinematic interaction (where soil filtering modifies input motion to the foundation) and inertial interaction (where superstructure inertia loads the foundation and dissipates energy into the soil) (Mylonakis et al. 1997; Guin & Banerjee, 1998; Forcellini, 2022; Islam et al. 2024), significantly altering system period and damping (Islam et al. 2024). Furthermore, structural embedment, a key design feature for stability, adds another layer of complexity. Embedment influences both kinematic interaction by altering wave paths and inertial interaction by mobilizing passive earth pressure, which can restrain pile head forces (Hu et al. 2024; Wang et al. 2024). While numerical studies suggest embedment generally enhances horizontal seismic safety (Hu et al. 2024; Wang et al. 2024), its specific effects within the context of piled raft foundations for full-scale NPPs, particularly through experimental validation, are not well established. Existing research lacks comprehensive large-scale experimental data quantifying the combined influence of piled raft foundations and structural embedment on the seismic response of critical NPP components (external plant, containment vessel, core equipment) in representative non-rock site conditions.

To address these critical research gaps, this study presents a series of novel large-scale shaking table tests. The experimental program uniquely compares the seismic performance of a nuclear reactor building model supported on three distinct foundation configurations representative of different site conditions and design strategies: (i) a fixed raft foundation (simulating rock sites), (ii) a piled raft foundation without structural embedment, and (iii) a piled raft foundation with structural embedment. By systematically analyzing seismic acceleration responses and response spectrum amplification characteristics across the model structure under various earthquake inputs, this research directly evaluates the SPSI mechanisms, quantifies the filtering effect of piled rafts in non-rock sites, and isolates the specific contribution of structural embedment to reducing seismic demands. The findings provide essential experimental benchmarks for validating SPSI theoretical and numerical models and deliver crucial insights for the safe seismic design of NPPs on non-rock sites globally.

2 EXPERIMENTAL EQUIPMENT AND RESEARCH SCHEME

2.1 *Large-scale shaking table facility*

This study utilized a large-scale seismic simulation shaking table facility developed by SERVOTEST Systems Ltd., UK. As shown in Figure 1, the table measures 6.0 × 9.0 m (expandable to 9.0 × 9.0 m), with a maximum payload capacity of 120 tons. It is equipped with a triaxial six-degree-of-freedom high-performance hydraulic actuator system and a Pulsar digital control system, capable of simulating near-fault ground motions. This facility integrates a non-contact three-dimensional dynamic deformation monitoring system, representing the world's first shaking table enabling full-process observation of structural seismic collapse. Additionally, the facility employs a Pacific Instruments 6000 data acquisition system coupled with a customized 256-channel testing and analysis system. This setup supports synchronous acquisition of multiple physical quantities including accelerations, pore water pressures, earth pressures, and displacements etc. The system achieves a maximum sampling rate of 200 kS/s per channel and a total sampling rate of 4 MS/s. High-precision synchronous acquisition and transmission of sensor signals are facilitated via a YS6000 junction box. Key technical parameters of the large-scale shaking table are summarized in Table 1.

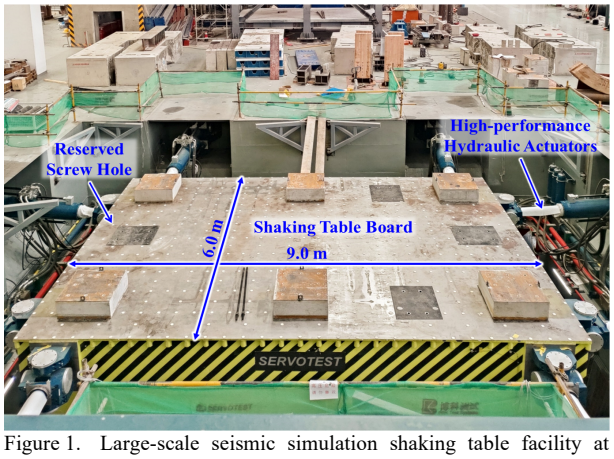

Figure 1. Large-scale seismic simulation shaking table facility at Southeast University

Table 1. The main technical parameters of large-scale seismic simulation shaking table.

Item name	Measurement range
Table size	6.0 m × 9.0 m (expandable to 9.0 m × 9.0 m)
Vibration direction	Three directions and six degrees-of-freedoms (X/Y/Z)
Maximum load	120 t
Maximum displacement	X/Y: +/-500 mm; Z: +/-300 mm
Maximum acceleration at full load	X/Y: 1.5 g; Z: 1.3 g
Maximum overturn moment	X/Y: 6,707 kN·m; Y: 6,391 kN·m (Meet simultaneously at maximum load)
Maximum eccentric moment	1,500 kN·m
Maximum eccentricity	±1.25 m
Operation frequency range	0.1 ~ 50 Hz
Vibration waveform	Periodic wave/random wave/seismic wave
Control mode	Pulsar digital control system
Pacific 6000 data acquisition system	256 Channels

2.2 *Innovative multi-directional laminar shear soil container*

An innovative multi-directional laminar shear soil container, designed specifically for this research, is shown in Figure 2. The rectangular container has dimensions of 5600 mm × 3800 mm × 2200 mm and can hold over 80 tons of test soil. The container body consists of 18 stacked rectangular hollow steel frames. Ball-bearing rollers installed between layers allow free relative displacement within the horizontal plane, with a vertical interlayer spacing of 23 mm. The container stiffness can be actively controlled to mitigate boundary effects and approximate semi-infinite foundation conditions by adjusting the number, diameter, and stiffness of energy-dissipating rods mounted on the outer walls. An external protective frame provides vertical restraint and horizontal displacement constraints. This frame, combined with interlayer limit rings and the energy-dissipating rods, forms a triple safety protection system for shaking table tests. Further details regarding this novel soil container can be found in Reference (Feng et al. 2025).

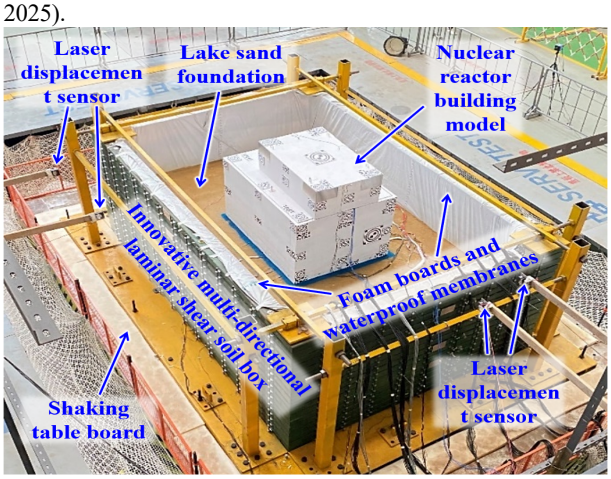

Figure 2. Innovative multi-directional laminar shear soil box.

Table 2 Similarity relationships between the test model and the actual prototype.

Type	Physical quantity	General similarity relation	Structure model (1g)	Ground soil model (1g)
Geometrical dimension	Length, L (m)	$n_L = (n_L)_m/(n_L)_p$	1/40	1/40
	Displacement, s (m)	$n_s = n_L n_\varepsilon$	1.975×10^{-3}	1.975×10^{-3}
Material property	Density, ρ (kg/m^3)	$n_\rho = (n_\rho)_m/(n_\rho)_p$	1	1
	Mass, M (kg)	$n_M = n_\rho(n_L)^3$	1/64000	1/64000
	Elasticity modulus, E (MPa)	$n_E = n_L n_\rho/n_\varepsilon$	0.316	0.316
	Soil tangent modulus, G (MPa)	$n_G = n_L n_\rho/n_\varepsilon$	—	0.316
	Soil shear velocity, v_s (m/s)	$n_{vs} = (n_{vs})_m/(n_{vs})_p$	—	0.563
Dynamic property	Acceleration, g (m/s^2)	$n_g = (n_g)_m/(n_g)_p$	1	1
	Time, t (s)	$n_t = (n_L)^{0.5}$	0.158	0.158
	Frequency, f (Hz)	$n_f = 1/n_t$	6.329	6.329
	Stress, σ (kPa)	$n_\sigma = n_L n_\rho$	1/40	1/40
	Strain, ε (%)	$n_\varepsilon = n_L(n_{vs})^{-2}$	0.079	0.079
	Force, F (kN)	$n_F = n_\rho n_g(n_L)^3$	1/64000	1/64000

2.3 *Shaking table test groups*

To investigate the influence of different foundation types on the seismic response of the nuclear island building, three sets of large-scale shaking table model tests were conducted:

(i) Fixed raft foundation model test (Case 1);

(ii) Piled raft foundation model test without embedment (Case 2);

(iii) Piled raft foundation model test with embedment (Case 3).

Similarity relationships governing model design were established through dimensional analysis (Iai, 1989; Wood, 2017), where Table 2 details derived scaling ratios. Comprehensive fabrication methodologies for each scaled model components of nuclear reactor building are documented in (Feng et al. 2025).

These tests enable an in-depth study of the influence mechanisms of foundation type and embedment depth on the seismic response characteristics of the nuclear island building. The test schemes are described below.

2.3.1 *Fixed raft foundation model test (case 1)*

The fixed raft foundation model test (Case 1) was performed to study the seismic response characteristics of the nuclear island building founded directly on bedrock. A schematic of the test model is shown in Figure 3. In this model, the nuclear island building base slab was rigidly fixed to the raft foundation. The raft foundation itself was rigidly secured to the shaking table platform via restraint keys installed around its perimeter, simulating the monolithic cast-in-place rigid connection between the nuclear island building and bedrock in actual engineering practice.

High-precision triaxial accelerometers were installed at the center of shaking table platform (No. A) and at the top of nuclear island building model (No. C), etc. These sensors monitored the time histories of input acceleration at the table and the structural top acceleration, respectively, during seismic excitation.

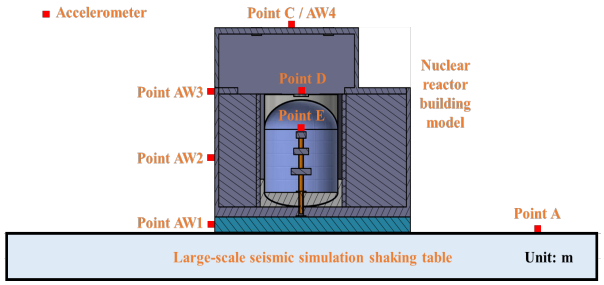

Figure 3. Schematic diagram of fixed raft foundation model (Case 1)

2.3.2 *Piled raft foundation model test without embedment (case 2)*

The model test of piled raft foundation without embedment (Case 2) was conducted to investigate the influence of a pile group foundation in non-rock sites on the seismic response of the nuclear island building. A schematic of the test model is shown in Figure 4.

The innovative multi-directional laminar shear soil container was bolted to the shaking table platform. The container, constructed from stacked rectangular steel tube frames, featured energy-dissipating rods mounted on its outer walls and was secured within an external protective frame to ensure test safety. After lining the inner walls of the container with foam panels and an impermeable membrane, natural lake sand, prepared to specific density and moisture content, was compacted in layers to a thickness of 1100 mm. During the sand placement process, a 4×5 array (20 total) of model aluminum tube piles was installed. The pile tips were positioned 200 mm above the container base. Following the completion of sand placement and pile installation, the cushion cap and nuclear island building model were installed. The pile tops protruded through the cap and were rigidly connected to the nuclear island building base slab via bolts.

High-precision triaxial accelerometers were installed at the center of the shaking table platform (No. A), within the soil between piles beneath the cushion cap (No. B), at the top of nuclear island building model (No. C / AW4), and at different heights along the building exterior wall (No. AW1~3). These sensors monitored the acceleration time histories at their respective locations.

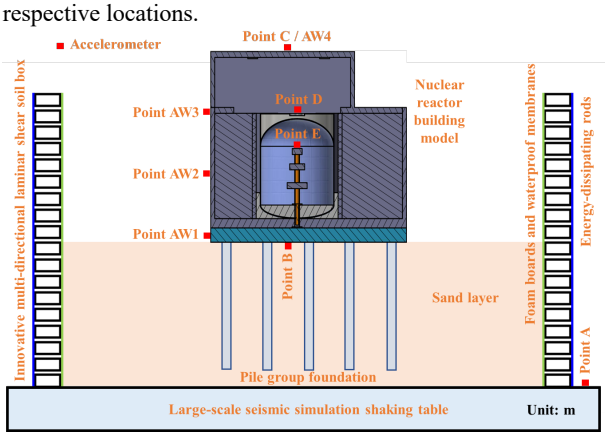

Figure 4. Shaking table test for piled raft foundation model without embedment (Case 2).

2.3.3 *Piled raft foundation model with embedment (case 3)*

The model test of piled raft foundation with embedment (Case 3) was performed to study the influence of the pile group foundation and its deep embedment condition on the seismic response of nuclear island building in non-rock sites. A schematic of the test model is shown in Figure 5.

Compared to Case 2, this test incorporated an additional layer of natural clay above the natural lake sand layer. The clay layer was also compacted in layers to achieve predetermined natural moisture content and density, with a placement thickness of 1000 mm. The installation methods for the model piles, cushion cap, and nuclear island building were identical to those described for the Case 2 test. The locations (No. A, B, C, and AW1~4) and functions of the accelerometers were also consistent with Section 2.3.2.

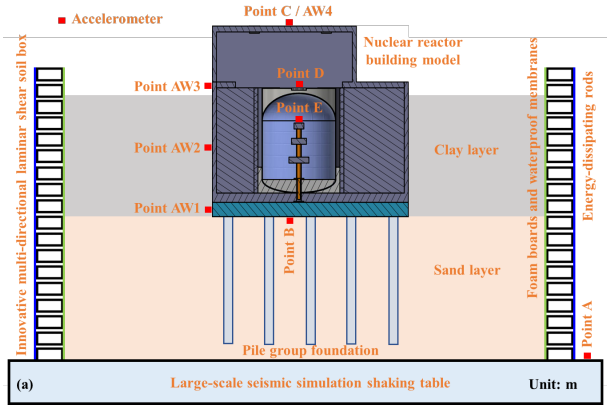

Figure 5. Shaking table test for piled raft foundation model with embedment (Case 3).

2.4 *Test loading protocol*

To achieve the research objectives, three distinct ground motion inputs were applied to each shaking table model test group, corresponding to the El Centro record (EL), an artificial synthetic record (RG), and the Chi-Chi record (CC). Specific

test conditions and the loading scheme are detailed in Table 3. To monitor the influence of seismic loading on the dynamic characteristics of the model structure, white noise (WN) excitation with a peak acceleration of 0.05 g was applied before and after each ground motion input for frequency sweep analysis. Each ground motion (including white noise) was input along three mutually perpendicular directions (X, Y, and Z).

Taking the Case 2 test as an example, Figure 6 presents the input acceleration time histories at the model base and their corresponding acceleration response spectra (with damping ratio uniformly set to 5%) under different ground motions. The acceleration monitored at the center of the shaking table platform (No. A) represents the input ground motion at the model base.

Table 3 Test conditions and peak value of output seismic acceleration.

Test group	Number	Seismic wave type	Vibration direction	Output acceleration peak on shaking table surface, a_{peak} (kPa)
Fixed raft foundation	WN1	White noise	X+Y+Z	X: 0.050 g; Y: 0.050 g; Z: 0.050 g
	EL1	EL-Centro wave		X: 0.410 g; Y: 0.468 g; Z: 0.212 g
	RG1	Artificial wave		X: 0.438 g; Y: 0.449 g; Z: 0.369 g
	CC1	Chi-Chi wave		X: 0.407 g; Y: 0.524 g; Z: 0.388 g
	WN2	White noise		X: 0.050 g; Y: 0.050 g; Z: 0.050 g
Piled raft foundation without embedment	WN3	White noise	X+Y+Z	X: 0.050 g; Y: 0.050 g; Z: 0.050 g
	EL2	EL-Centro wave		X: 0.329 g; Y: 0.265 g; Z: 0.373 g
	RG2	Chi-Chi wave		X: 0.451 g; Y: 0.379 g; Z: 0.608 g
	CC2	Artificial wave		X: 0.257 g; Y: 0.348 g; Z: 0.495 g
	WN4	White noise		X: 0.050 g; Y: 0.050 g; Z: 0.050 g
Piled raft foundation with embedment	WN6	White noise	X+Y+Z	X: 0.050 g; Y: 0.050 g; Z: 0.050 g
	EL3	EL-Centro wave		X: 0.350 g; Y: 0.271 g; Z: 0.186 g
	RG3	Chi-Chi wave		X: 0.396 g; Y: 0.379 g; Z: 0.312 g
	CC3	Artificial wave		X: 0.325 g; Y: 0.318 g; Z: 0.273 g
	WN6	White noise		X: 0.050 g; Y: 0.050 g; Z: 0.050 g

As shown in sub-figure 6 (a), for the EL input, the spectral characteristics in the X- and Y-directions were similar. The predominant structural periods corresponding to the spectral peaks were 0.070 s and 0.072 s, respectively, which are close in value. The spectral characteristics in the Z-direction differed significantly from the horizontal directions, and its predominant structural period (0.024 s) was notably shorter. sub-figure 6 (b) indicates that for the RG input, the spectral characteristics exhibited some differences between the X- and Y-directions, with predominant structural periods of 0.068 s and 0.058 s, respectively. Furthermore, the spectral values in the Z-direction were significantly higher than in the horizontal directions, although its predominant structural period (0.050 s) was still shorter than those in X- and Y-directions. As seen in sub-figure 6 (c), for the CC input, the spectral characteristics differed considerably between X- and Y-directions. The predominant structural period in the X-direction (0.076 s) was longer than in the Y-direction (0.054 s). The spectral values in the Z-direction were again significantly higher than the horizontal values, while its predominant period (0.050 s) was close to that of the Y-direction.

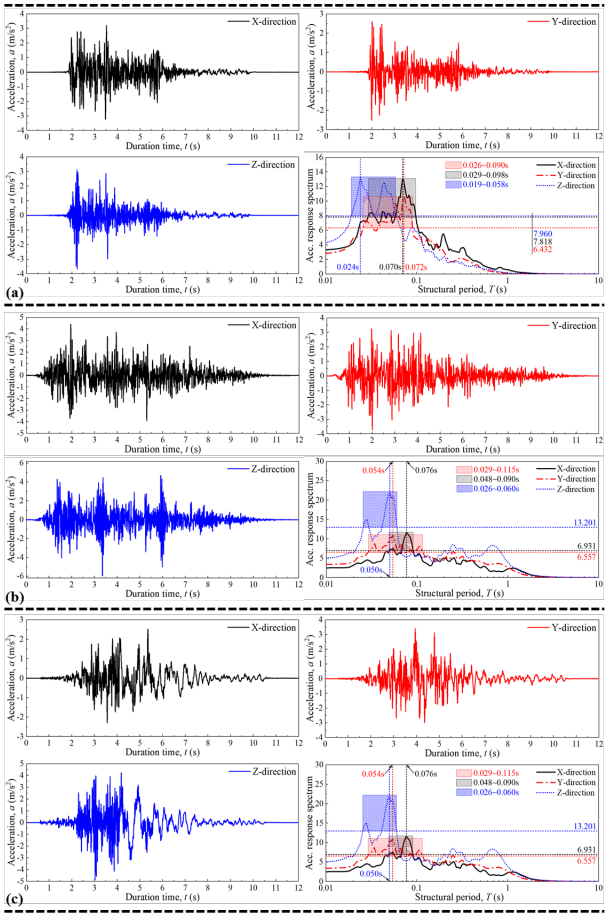

Figure 6. Input acceleration time histories and response spectrum for Case 2 model test monitored at the model base (No. A): (a) EL; (b) AS; and (c) CC.

Comparative analysis of the acceleration response spectra for the three ground motions in Figure 6 yields the following key features: (i) For the EL motion, the region of higher spectral values was concentrated in the short-to-medium structural period (medium-to-high frequency) range, exhibiting a relatively broad bandwidth. (ii) For the RG motion, the region of higher spectral values was primarily located in the medium structural period (medium frequency) range, with a narrower bandwidth. The Z-direction spectral values were significantly higher than the horizontal values. (iii) For the CC motion, the region of higher spectral values covered short, medium, and long structural periods (high, medium, and low frequencies), showing the broadest bandwidth. The Z-direction spectral values were also significantly higher than the horizontal values.

In summary, the three selected ground motion inputs possess distinct spectral characteristics, providing suitable excitation conditions for investigating the influence of ground motions with different spectral features on the seismic response of the pile-supported nuclear island building.

3 COMPARATIVE ANALYSIS OF SEISMIC RESPONSE OF NUCLEAR ISLAND BUILDING ON DIFFERENT FOUNDATIONS

Based on three sets of large-scale shaking table tests (Cases 1, 2, and 3), a comparative analysis was conducted to investigate the influence of different foundation conditions on the seismic response of the upper nuclear island building. The study specifically focused on the mechanisms by which key factors—namely foundation type, embedment condition, and ground motion type—affect the acceleration response characteristics at various locations of the nuclear island building. To this end, the comprehensive amplification factors of peak acceleration for all monitoring points on the test model relative to the shaking table platform and the model base (top of the pile group foundation) were summarized. Differences in the corresponding acceleration response spectra were also comparatively analyzed.

3.1 *Acceleration Amplification Effect of Nuclear Island Building*

To quantitatively assess the impact of different foundation conditions, the comprehensive amplification factors of peak acceleration for the tops of key components of the nuclear island building model (point C at the top of the external building, point D at the top of the nuclear equipment inside the containment vessel, and point E at the top of the containment vessel) relative to the shaking table platform (point A) and the model base (point B) were statistically analyzed; the results are detailed in Table 4.

Table 4 Comprehensive peak acceleration amplification factors of nuclear island building model on different foundations.

Model type	Reference monitoring point (A/B)	Overall amplification factors of peak acceleration	Mean value
Fixed raft foundation	Shaking table surface/Model base (A/B)	2.523	2.523
Piled raft foundation without embedment	Shaking table surface (A)	2.446	2.145
	Model base (B)	1.844	
Piled raft foundation with embedment	Shaking table surface (A)	2.006	1.891
	Model base (B)	1.632	

Analysis of Table 4 data reveals that, regardless of the reference point (A or B), and under the three seismic loads (EL, RG, CC), the comprehensive amplification factors of peak acceleration for all monitoring points in the upper nuclear island building consistently follow the same order: Case 1 > Case 2 > Case 3. Specifically, relative to reference points A and B:

(i) The comprehensive peak acceleration amplification factors for the piled raft foundation model without embedment were reduced by 3.05% and 26.91%, respectively, compared to the fixed raft foundation model, yielding an average reduction of 14.98%.

(ii) The comprehensive peak acceleration amplification factors for the piled raft foundation model with embedment were reduced by 20.49% and 35.32%, respectively, compared to the fixed raft foundation model, yielding an average reduction of 27.91%.

This indicates that employing a piled raft foundation, especially with embedment, on non-rock sites provides significant advantages in suppressing the overall acceleration amplification effect of the upper nuclear island building. This advantage is particularly pronounced when the ground motion input at the raft base is used as the reference.

3.2 *Characteristics of acceleration response spectra for nuclear island building*

Furthermore, to elucidate the influence of foundation type on the overall spectral characteristics of seismic acceleration for the nuclear island building, Figure 7 presents the variation curves of the comprehensive amplification factors for tri-directional acceleration response spectral amplitudes (relative to points A and B) at all measurement points (points C, D and E) with structural period, under different foundation conditions.

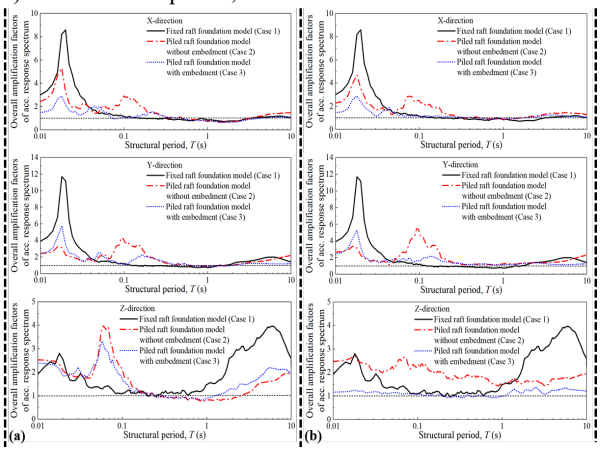

Figure 7. Variation of overall amplification factors of 3D acceleration response spectrum amplitudes at the top monitoring points with structural period relative to: (a) shaking table surface; and (b) model base.

Analysis of sub-figure 7 (a) shows that the foundation type significantly alters the shape of the acceleration response spectral amplification factor curves for the building structure. In the horizontal directions (X or Y), compared to the fixed raft foundation, the piled raft foundation effectively reduced the spectral amplification effect near structural resonance periods, and the embedment condition further suppressed this effect. Particularly in Y-direction, while the piled raft foundation exhibited higher amplitude at the first resonance period, it demonstrated a pronounced suppression effect near the second resonance period. In the vertical direction (Z), all three foundation types exhibited high amplification effects in the low and high structural period ranges, but the curve for piled raft foundation with embedment was the lowest overall. Notably, in the low structural period range, the resonance period value for piled raft foundation was higher than that for fixed raft foundation, while in the high period range, the spectral amplitude of the former was lower than that of the latter.

Analysis of sub-figure 7 (b) reveals that the shapes of the horizontal (X or Y) response spectral curves are essentially consistent with those relative to the shaking table platform. However, in the vertical direction (Z), the piled raft foundation significantly reduced the response spectral amplification factors. Particularly, the curve for pile group foundation with embedment exhibited values close to 1 across the entire structural period range, nearly eliminating the vertical acceleration response spectral amplification effect in the superstructure.

Synthesis of the quantitative analyses of both peak acceleration amplification factors and acceleration response spectra demonstrates that piled raft foundation conditions

(especially pile-raft foundation with embedment), compared to the fixed raft foundation, significantly reduce the overall acceleration amplification effect of the nuclear island building structure. This conclusion holds true for different seismic loads and reference points. The underlying mechanism lies in the combined effects of SPSI and the lateral constraint provided by the surrounding soil under embedment conditions, which collectively dissipate seismic energy. This energy dissipation alters the dynamic characteristics of building structure, differentiating its seismic response from that of a nuclear island building founded on bedrock.

4 NUMERICAL SIMULATION STUDY ON SEISMIC RESPONSE OF PILE-SUPPORTED NUCLEAR ISLAND BUILDING

4.1 *Finite element modeling procedure*

To validate the effectiveness of the numerical simulation methodology for seismic response of the non-rock site–piled raft foundation–nuclear island building system, this study developed a 3D finite element model (FEM) based on the ABAQUS software platform. The FEM targeted the pile-raft foundation model without embedment used in the shaking table tests. Validation was achieved through comparative analysis of experimental and simulation results.

The modeling procedure encompassed the following steps:

Geometry creation: Based on the geometric parameters of the experimental model, solid elements were employed to create key components including the soil container, test soil, aluminum pipe pile group, concrete building structure, and steel containment vessel.

Model assembly: The individual components were assembled to form the complete nuclear island building test model, as illustrated in Figure 8.

Interaction definition: A normal "hard contact" and tangential "Penalty friction" contact model was assigned to the interface between the superstructure and the foundation soil. A similar "hard contact" with "Penalty friction" was also applied to the interface between the test soil and the soil container. All other component interfaces were simulated using "tie constraints".

Meshing: The steel containment vessel was meshed using a swept meshing technique. Structured meshing techniques were applied to all other components. The entire model utilized reduced-integration 8-node linear brick elements (C3D8R).

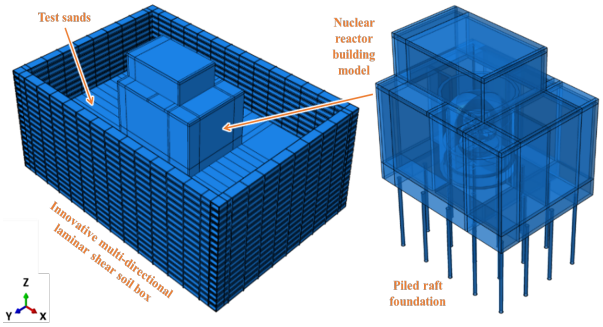

Figure 8. Finite element model of the pile-supported nuclear island building for large-scale shaking table test

4.2 *Validation of numerical simulation results for nuclear island building seismic response*

Figure 9 presents a comparison of the acceleration time histories obtained from the shaking table test and numerical simulation at various monitoring points of the pile-supported nuclear island building model (Note: Valid test data for point AWY3 was unavailable due to accelerometer malfunction).

Comparative analysis reveals:

Waveform agreement: The acceleration time-history curves from the test and simulation exhibit a high degree of agreement in shape for all valid monitoring points, with peak accelerations occurring at essentially the same time instances.

Quantitative error: Error analysis shows maximum discrepancies in 3D peak accelerations of 10.17% (X-direction), 12.5% (Y-direction), and 20.04% (Z-direction). This indicates superior reliability of the FEM in simulating horizontal (X or Y) seismic responses compared to the vertical (Z) direction.

Amplification effect: Both experimental and simulation results demonstrate a significant seismic acceleration amplification effect – horizontal input acceleration amplifies progressively along the height of the nuclear island building. Peak acceleration errors at monitoring points of the same height are relatively small.

The observed consistency validates that the established FEM accurately simulates the acceleration amplification response characteristics of a pile-supported nuclear island building on non-rock sites. This provides a robust methodological foundation for subsequent parametric studies.

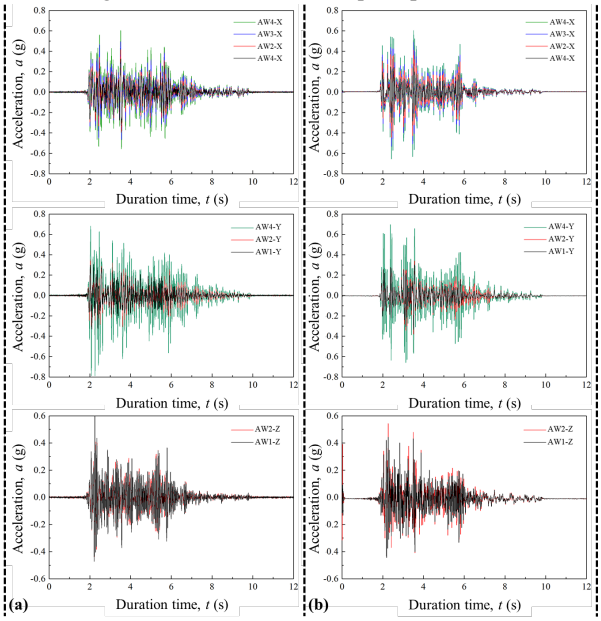

Figure 9. Comparison of acceleration time histories from shaking table test and numerical simulation for the pile-supported nuclear island building

4.3 *Analysis of bending moment response in pile group foundation*

Based on the elastic foundation beam theory, the bending moment (MM) at a pile cross-section is calculated from the tensile strain (ε_t) and compressive strain (ε_c) measured on opposite sides:

$$M = \frac{EI\left(\varepsilon_t - \varepsilon_c\right)}{2r}$$

Where: E is the elastic modulus of the pile material; I is the inertia moment of the pile cross-section; and r is the outer radius of the pile cross-section.

Figure 10 shows the experimental envelope of measured peak bending moments along the instrumented test piles under 0.4g EL excitation. Key experimental findings include:

Peak moment location: The maximum bending moment for each pile consistently occurs at the pile head. This phenomenon arises from the pronounced dynamic response

induced by the inertial forces of the superstructure, highlighting the dominant influence of structure-foundation interaction (SFI) at the pile head region.

Non-uniform distribution: The bending moment distribution across the pile group is non-uniform. Pile No. 1 exhibits the largest pile head moment, attributed directly to the spatial variability of compacted fill density and heterogeneous pile-soil contact conditions.

Load distribution pattern: Under strong seismic excitation, when the lateral bearing capacity of the pile group is fully mobilized, the load distribution follows the pattern: corner piles > edge piles and front-row piles > back-row piles.

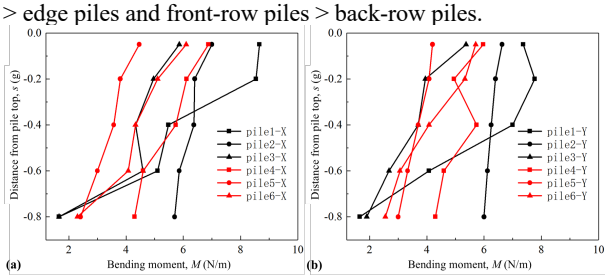

Figure 10. Experimental envelope of measured bending moments along instrumented test piles under 0.4g EL excitation: (a) X-direction; and (b) Y-direction.

For comparison, Figure 11 presents the envelope of peak bending moments along the pile group obtained from numerical simulation under the same 0.4g EL excitation (Note: The numerical model incorporated additional sampling points along the pile length to enhance accuracy). The simulation successfully replicates the core experimental trends:

Moment distribution: Peak moments exhibit an approximately "S-shaped" distribution along the pile length, with the maximum value at the pile head decreasing towards the pile tip.

Directional dominance: The increase in pile head moment is significantly higher in the X-direction compared to the Y-direction, indicating the dominance of inertial SPSI effects on the X-direction response under strong shaking.

Load distribution: The patterns "corner piles > edge piles > center piles" and "front-row piles > back-row piles" are clearly reproduced.

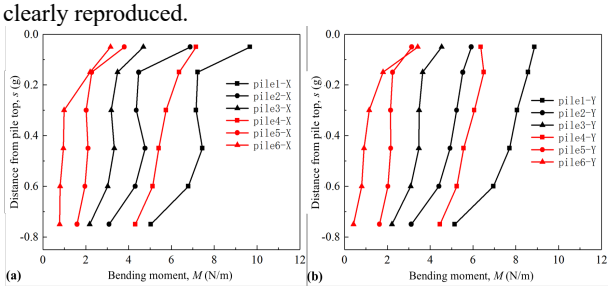

Figure 11. Numerical simulation envelope of bending moments along instrumented test piles under 0.4g EL excitation: (a) X-direction; and (b) Y-direction

However, discrepancies exist between the experimental and simulated maximum pile head moments for piles 1 to 6: 9.65%, 3.7%, 19.92%, 15.11%, 32.46%, and 25.21%, respectively. Errors exceeding 15% are observed for piles 3, 5, and 6. These discrepancies are primarily attributable to:

(i) The homogeneous soil assumption in the numerical model failing to capture the spatial variability of compacted fill density present in the test.

(ii) The idealized rigid connection between piles and the cushion cap potentially underestimating the actual response of center piles.

(iii) The FFM limitation in simulating the progressive development of pile group capacity, potentially leading to an overestimation of the load share on edge and corner piles compared to the test.

These differences underscore key challenges in numerically modeling the complex mechanisms of seismic SPSI.

Given the increasing scarcity of premium bedrock sites for nuclear power plants in China, the novel findings of this study hold significant engineering implications. The research confirms that employing deep embedded structure supported on pile-raft foundations in non-rock sites can effectively enhance the seismic performance of nuclear island buildings by significantly mitigating their seismic response. This provides crucial technical supports for the safe and efficient expansion of China's nuclear power engineering projects from bedrock to non-rock sites.

5 DISCUSSION

The significantly greater reduction in peak acceleration amplification factors observed for the embedded piled raft foundation (Case 3), particularly when referenced to the model base (Point B, 35.32% reduction compared to fixed raft), is probably attributed to the following synergistic mechanisms enhanced by the embedment depth, as evidenced by experimental and numerical results:

Embedment subjects the raft to significant passive soil pressure, substantially restricting its translational and rotational movement compared to surface foundations. This confinement impedes direct seismic energy transmission to the superstructure. Numerical simulations confirm an obvious increase in plastic strain energy dissipation within the soil surrounding the embedded raft edges, acting as a major energy sink. Experimentally, this is reflected in the drastically lower amplification at Point B for Case 3 (1.632) vs. Case 1 (2.523) and Case 2 (1.844) (Table 4).

The larger soil-structure interface area provided by embedment facilitates greater energy dissipation through friction and radiation damping, elevating the overall system damping ratio. Experimentally, acceleration response spectra (Figure 7) show a faster decay rate in the dominating structural frequency range for Case 3 vs. Case 2. Numerically, parametric studies show embedment increasing the equivalent viscous damping ratio. Furthermore, kinematic interaction places the foundation within the soil wave field, causing phase differences and filtering high-frequency input components.

These mechanisms – increased foundation restraint, enhanced damping, and high-frequency filtering – act together within the embedded piled raft system. They fundamentally alter the seismic energy pathway entering the structure, especially at the foundation level (Point B). This explains the embedded foundation's superior performance: achieving a substantially greater average reduction in amplification (27.91%, max 35.32% at Point B) compared to the surface-founded piled raft (14.98% average, max 26.91% at Point B). The advantage is most pronounced for input referenced to the raft base, as embedment modifies the motion before it excites the superstructure, offering significant benefits for nuclear buildings on non-rock sites.

While this study demonstrates that embedded piled raft foundations (e.g., at a prototype depth of 35 m) reduce peak acceleration amplification by up to 35.32% compared to fixed rafts, optimal embedment depth ratios require further parametric investigation. Preliminary observations suggest a depth of 0.45× foundation width or 1 time pile length as potentially effective for similar non-rock sites. Future work will quantify depth-to-

width/length ratios balancing seismic gains and constructability across varied soil profiles.

6 CONCLUSIONS

Through a series of large-scale shaking table tests conducted on scaled models of the nuclear island building on different foundations, a deeper understanding of the seismic response of the non-rock site–piled raft foundation–nuclear island building system has been achieved. The following key conclusions are drawn:

(1) An innovative multi-directional laminar shear soil container was developed. Based on the physical and mechanical properties of the test soil within the container, the design parameters of its energy-dissipating rods can be adjusted as required. This enables autonomous control of the container's stiffness, effectively minimizing the influence of boundary effects on test results and approximating the conditions of a semi-infinite foundation. Measurements confirmed a boundary effect index (μ) of less than 3.5% for the container.

(2) Soil-pile-structure interaction (SPSI) effectively reduces the seismic amplification effect in the nuclear island building compared to the condition of a fixed raft foundation on rigid bedrock. Measurements indicate a comprehensive reduction in the building's acceleration amplification factors ranging from 14.98% to 27.91%.

(3) Both experimental measurements and numerical simulation results demonstrate that under strong seismic excitation, when the lateral bearing capacity of the pile group foundation is fully mobilized, peak bending moments concentrate at the pile heads, and the load distribution follows distinct patterns: corner piles > edge piles > center piles, and front-row piles > back-row piles.

(4) For constructing nuclear power plants on non-rock sites, a piled raft foundation scheme with a certain structure embedment depth should be adopted. Utilizing the passive earth pressure constraints provided by the surrounding soil effectively reduces the vertical amplification effect of seismic action on the nuclear island building.

7 ACKNOWLEDGEMENT

The authors would like to gratefully acknowledge the supports from the Scientific Research Program of Shanghai Nuclear Engineering Research & Design Institute Co. Ltd. (SNERDI), National Natural Science Foundation of China (Grant Nos. 52378328 and 52178317), Postgraduate Research and Practice Innovation Program of Jiangsu Province (Grant No. KYCX22_0217), and the National Construction of High-level University Public Graduate Project (Grant No. CSC202206090133).

8 REFERENCES

American Society of Civil Engineers, 2017. ASCE/SEI 4-16: Seismic analysis of safety-related nuclear structures.

Clancy, P. and Randolph, M.F., 1993. An approximate analysis procedure for piled raft foundations. International Journal for Numerical and Analytical Methods in Geomechanics, 17(12), 849-869.

Feng, D., Zhu, W.B., Chu, M., et al., 2025. Application of innovative multi-directional laminar shear box to evaluate seismic soil – Pile foundation – Nuclear power plant interaction. Soil Dynamics and Earthquake Engineering, 190, 109152.

Forcellini, D., 2022. Seismic fragility of tall buildings considering soil structure interaction (SSI) effects. Structures, 45, 999-1011.

Forcellini, D., 2023. The role of Soil Structure Interaction (SSI) on the risk of pounding between low-rise buildings. Structures, 56, 05014.

Guin, J. and Banerjee, P.K., 1998. Coupled soil-pile-structure interaction analysis under seismic excitation. Journal of Structure Engineering, ASCE, 124(4), 434-444.

Hu, Z.W., Li, J.B. and Lin, G., 2024. Study on seismic performance and embedded effects on reactor buildings cluster considering nonlinear structure-soil-structure interaction. Journal of Building Engineering, 97, 110911.

Hu, Z.W., Li, J.B. and Lin, G., 2025. Seismic nonlinear interaction and uplifting effects between the nuclear island building and soil. Engineering Structures, 322(Part B), 119168.

IAEA, 2015. Fukushima Daiichi Accident – Report by the IAEA Director General. IAEA Non-serial Publications.

IAEA, 2016. Geotechnical Aspects of Site Evaluation and Foundation for Nuclear Power Plants. IAEA Safety Standards Series, No. NS-G-3.6.

Iai, S., 1989. Similitude for shaking table tests on soil-structure-fluid model in 1g gravitational field. Soils and Foundations, 29(1), 105-118.

Islam, M.R., Turja, S.D., Nguyen, D.V., et al., 2024. Seismic soil-structure interaction in nuclear power plants: An extensive review. Results in Engineering, 23, 102694.

Liu, Y., Li, J.B. and Lin, G., 2024. Nonlinear numerical study of structure-soil-structure interaction effects between conventional and three-dimensional base-isolated nuclear power plants. Soil Dynamics and Earthquake Engineering, 187, 108985.

Maruyama, H., Santa, M.S., Kato, H., et al., 2010. Nonlinear Soil Behavior Observed at Vertical Array in the Kashiwazaki-Kariwa Nuclear Power Plant during the 2007 Niigata-ken Chuetsu-oki Earthquake. Bulletin of the Seismological Society of America, 100(2), 762-775.

Martin, P.G., 2018. The 2011 Fukushima Daiichi Nuclear Power Plant Accident – An Analysis from the Metre to the Nanometre Scale. Springer International Publishing AG.

Ministry of Housing and Urban-Rural Development of the People's Republic of China, 2014. Code for Geotechnical Investigation of Nuclear Power Plants, GB 51041-2014.

Mostafa, Y.E. and El Naggar, M.H., 2002. Dynamic analysis of laterally loaded pile groups in sand and clay. Canadian Geotechnical Journal, 39(6), 1358-1383.

Mylonakis, G., Nikolaou, A. and Gazetas, G., 1997. Soil-pile-bridge seismic interaction: Kinematic and inertial effects. 1. Soft soil. Earthquake Engineering & Structural Dynamics, 26(3), 337-359.

Poulos, H.G. and Davids, A.J., 2005. Foundation design for the emirates twin towers, Dubai. Canadian Geotechnical Journal, 42(3), 716-730.

Sonoda, R., Matsumoto, T., Kitiyodom, P., et al., 2009. Case study of a piled raft foundation constructed using a reverse construction method and its post-analysis. Canadian Geotechnical Journal, 46(2), 142-159.

Tang, A.K. and Schiff, A.J., 2010. Kashiwazaki, Japan, earthquake of July 16, 2007: lifeline performance. SciTech Book News.

Uetake T, Tokumitsu R, Nishimura I, et al. Effects of fold structure in the kashiwazaki-kariwa nuclear power station on the ground motion characteristics of Niigataken Chuetsu-Oki Earthquake – Modeling of sub-surface structure and wave propagation study using a finite difference method. Journal of Structural and Construction Engineering 2011; 76 (660): 311-318.

Wang, X., Zhao, M., Guan, J.C., et al., 2024. Site effect on seismic response of buried nuclear power plant structure. Soil Dynamics and Earthquake Engineering, 183, 108759.

Westinghouse Electric Company LLC, 2007. Chapter 3, of Structures, Components, Equipment and Systems, AP1000 Design Control Document, Rev.16.

Wood, D.M., 2017. Geotechnical modelling. CRC Press. Yang, Y., Gong, W., Cheng, Y.P., et al., 2021. Effect of soil-pile-structure interaction on seismic behaviour of nuclear power station via shaking table tests. Structures, 33, 2990-3001.

Yin, H.F., Bo, J.H. and Li, P., 2015. Study on seismic responses of soft rock subgrade for a nuclear power plan. Earthquake Engineering and Engineering Dynamics, 35(01), 44-49.

Zou, D., Sui, Y. and Chen, K., 2020. Plastic damage analysis of pile foundation of nuclear power plants under beyond-design basis earthquake excitation. Soil Dynamics and Earthquake Engineering, 136(2), 106179.